A Monte Carlo based phase space model for quality assurance of intensity modulated radiotherapy incorporating leaf specific characteristics

Randi F. Aaronson[a)] and John J. DeMarco
Department of Radiation Oncology, University of California, Los Angeles, California 90095-6951

Indrin J. Chetty
Department of Radiation Oncology, University of Michigan, UHB2C438 Box 0010, Ann Arbor, Michigan 48109-0010

Timothy D. Solberg
Department of Radiation Oncology, University of California, Los Angeles, California 90095-6951

(Received 4 September 2002; accepted for publication 30 September 2002; published 3 December 2002)

Dose calculations for intensity modulated radiation therapy (IMRT) require an accurate description of the radiation field defined by the multileaf collimator. A previously developed Monte Carlo phase space model has been modified to provide accurate dose verification for IMRT treatments on a Novalis linear accelerator. We have incorporated into the model the effects of the multileaf collimator geometry, including leaf transmission, interleaf leakage, the rounded leaf tips and the effects of leaf sequencing, as well as the beam divergence and energy variation across the field. The modified source model was benchmarked against standard depth dose and profile measurements, and the agreement between the calculation and measurement is within the AAPM Task Group No. 53 criteria for all benchmark fields used. Film dosimetry was used to evaluate the model for IMRT sequences and plans, and the ability of the model to account for leaf sequencing effects is also demonstrated.
[DOI: 10.1118/1.1523409]

Key words: IMRT treatment plan verification, intensity modulated radiotherapy, Monte Carlo, multileaf collimator

I. INTRODUCTION

The development of more advanced treatment modalities in radiation therapy, such as intensity modulation, brings a need for increasingly sophisticated quality assurance techniques. Intensity modulated radiation therapy (IMRT) involves a series of small shaped fields resulting in complex intensity distributions, which limits the effectiveness of traditional verification methods. For accurate dose calculations, IMRT requires a model that is able to simulate complex and arbitrary fluence maps and account for electronic disequilibrium due to heterogeneities and surface irregularities.

Commonly used verification techniques, including radiographic film and electronic portal imaging devices, can be labor-intensive processes. Although direct measurements are accurate, computational verification is a more efficient technique. Most conventional calculation algorithms, however, do not account for electron transport; therefore they do not accurately predict dose in small fields where lateral electronic equilibrium is not achieved. The IMRT Collaborative Working Group[1] presents a set of recommendations for dose verification of IMRT. They suggest that all IMRT dose-calculation algorithms model the finite source size, extra focal radiation and electron contamination. In contrast to the other common techniques, the Monte Carlo method starts from first principles and tracks individual particle histories, thus it takes into account the transport of secondary particles and also the electronic disequilibrium present in small fields. The Monte Carlo method produces accurate results in regions of tissue heterogeneities and surface irregularities, providing the most convenient and accurate method for the simulation of patient-specific treatment distributions.[2–7]

The dynamic nature of IMRT treatments introduces verification issues that are not present or not significant in conventional radiation therapy. Because of the numerous small fields used in IMRT, the intensity distributions are more complex than for static shaped beams. The well-documented effects of the shaped leaf tips and the tongue-and-groove geometry are much more significant in IMRT, and have been shown to contribute 10–15% of the maximum in-field dose.[8–10] In a computational model of the multileaf collimator (MLC), the Collaborative Working Group advises considering the "effects of MLC leaf leakage, leaf transmission, ... leaf side and end transmission, and the effects of leaf sequencing."[1]

Three other groups have described integrated Monte Carlo models for IMRT simulation. In their paper, Fix *et al.*[11] describe the application of a multiple source model to IMRT. This model transports particles through the MLC accounting for the tongue-and-groove, but approximating the shaped tip of the leaves. Pawlicki and Ma[12] use an intensity grid in their simulation, which is more efficient than modeling and transporting particles through the individual leaves. However they only consider the average leaf transmission, ignoring the specific geometry of the MLC. In the method described by Keall *et al.*[13] the path length through the MLC is calculated for each incident photon, accounting for the specific geometries of the MLC, beam divergence, the energy variation across the field and an approximation of the first Compton scatter.

In this paper we describe the modifications to a previously developed phase space source model, which incorporate the necessary features for accurate Monte Carlo based verification of IMRT fields using a Novalis linear accelerator. The phase space model, as described by Chetty *et al.*,[14,15] employs a treatment-specific intensity grid to adjust the open beam fluence map for arbitrarily shaped fields. This is an efficient method for simulating IMRT beams because the intensity grid is created in a preprocessing calculation, and it does not require transporting particles through the field defining collimators. The modifications we have made to the model include the ability to simulate series of fields, as used in IMRT, and to account for the tongue-and-groove and shaped leaf tip geometries of the multileaf collimator, the divergence of the beam and the energy variation across the field. The applications of this model include patient quality assurance, commissioning treatment planning systems and evaluating leaf-sequencing algorithms. We will demonstrate the accuracy of the model and it's usefulness in evaluating leaf-sequencing effects and as a quality assurance tool for IMRT.

II. MATERIALS AND METHODS

A. Accelerator design

A Novalis 6 MV linear accelerator (BrainLAB AG, Heimstetten, Germany) was used for this study. It was originally designed as a dedicated shaped beam system for stereotactic radiosurgery, therefore it incorporates a wide output range and high rotational accuracy. Novalis is equipped with a micro-multileaf collimator, m3 mMLC (BrainLAB AG, Heimstetten Germany and Varian Oncology Systems, Palo Alto, CA) with a maximum field size of 10×10 cm^2 at the isocenter. While the field size is limiting, it has been found to be appropriate for many common IMRT targets, such as prostate boost and head-and-neck treatments. The m3 has narrow leaves to provide improved conformity to small targets, as compared with conventional collimators, making Novalis an excellent system for select IMRT treatments.

The m3 collimator has 26 pairs of tungsten alloy leaves, with widths of 3 mm, 4.5 mm, and 5.5 mm, projected at isocenter. The leaves are linearly mounted with the center at a distance of 55.5 cm from the source, and they are focused to converge at the source. The collimator incorporates the tongue-and-groove design to reduce interleaf leakage, and the leaves have a shaped tip in the vertical direction to produce an approximately constant penumbra at the isocenter. The full overtravel and interdigitation capabilities of the collimator eliminate leakage between an opposing pair of closed leaves because the junction is moved under the backup jaws. Leaf transmission for this system has been measured to be approximately 1.3%, and interleaf transmission is between 1.6% and 2.1%, which is consistent with the analyses of Xia *et al.*[16] and Cosgrove *et al.*[17] The Novalis system can operate in either dynamic or step-and-shoot mode, however the simulation model currently supports only step-and-shoot delivery.

B. The phase space model

A phase space model has previously been developed for the simulation of arbitrary intensity distributions for conventional clinical treatment planning.[14,18,19] The basis of development for the model is the MCNP4C (*M*onte *C*arlo *N*-*P*article, version 4C) code,[20] which is a coupled neutral/charged particle code. The code uses a three dimensional heterogeneous geometry and transports photons and electrons in the energy range from 1 keV to 100 MeV. Low energy phenomena, such as characteristic x-rays and Auger electrons, are also accurately modeled. MCNP requires the source for a particular problem to be specified in a user-defined input file. The source includes distributions of the position, energy and angle of starting particles. For this work, the phase space source is supplied by a patch file, which was developed using standard Fortran code and the PRPR pre-processor that is included in the MCNP4C distribution package.

1. Acquisition of fluence distribution

The phase space is created by calculating the fluence of an open beam, and then adjusting that fluence to match an arbitrary field shape. The open beam fluence is determined by simulating the components of the linear accelerator treatment head above the field defining collimators, using the MCNP4C code. The tally plane for this simulation is located 50 cm below the target, which is under the macro-jaws, but above the multileaf collimator. The tally consists of MCNP point and ring detectors, which score relative photon fluence. Nineteen ring detectors are placed at equal intervals extending radially outward from a point detector on the central axis. The tally covers a circular region of diameter 7 cm, corresponding to 14 cm diameter at isocenter, which covers the 10×10 cm^2 maximum field size. The fluence distributions for the open beam are then reconstructed into a 200×200 pixel Cartesian grid with discrete photon fluence elements, in a process previously described by Chetty *et al.*;[15] each pixel has dimensions of 0.5×0.5 mm^2 at the isocenter.

By modeling the treatment head above the field defining collimators, the resulting fluence values are patient-independent and thus only need to be calculated once. This virtual source description is used for all subsequent simulations, including benchmarks and IMRT plans with a series of shaped fields. During the simulation, the starting particle's position (x,y) is sampled from the fluence map. The radial distance $[R=(x^2+y^2)^{0.5}]$ is calculated, and the particle's energy is sampled from the energy distribution of the bin that is closest to R. The angular dependence is based upon a point source model at the position of the linear accelerator target.

2. Analysis of fluence distribution

The conical shape of the flattening filter causes a preferential attenuation of lower energy photons toward the center

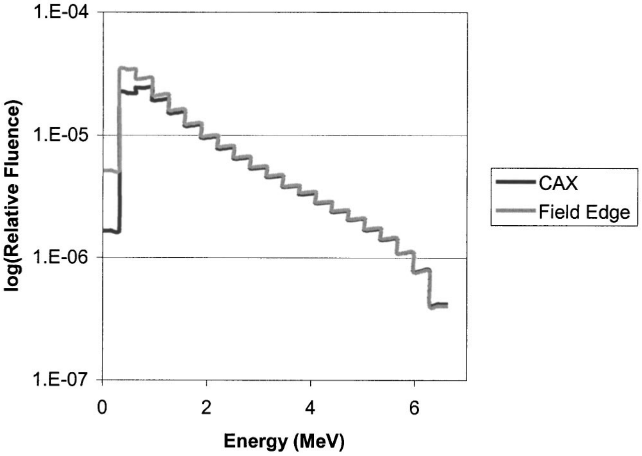

FIG. 1. Bremsstrahlung spectra for point and ring detectors located at the central axis and near the edge of the field ($R=4.78$ cm at isocenter). The corresponding mean energies are 1.82 MeV at the central axis and 1.66 MeV at the field edge.

of the field. This results in a relative increase in the integrated photon fluence at the edge of the field with respect to the center, and a corresponding decrease in the average energy. Figure 1 illustrates the bremsstrahlung spectra for the central axis as well as near the edge of the field. There is an increase in the integrated fluence of 19% and a decrease in the mean energy of 8.8% from the central axis to the edge of the field.

While the point source approximation underestimates the extra-focal component of the photon output, the limited field size of 10×10 cm^2 and the small flattening filter of the Novalis accelerator minimizes the effects of the finite source size and location. An analysis of the fluence contribution from the various structures in the treatment head shows that at the isocenter, approximately 97% of the fluence is from the target, and 1.2% from the flattening filter. This is much lower than the flattening filter fluence contribution at isocenter of 2.5% reported by Chaney *et al.*[21] for a 6 MV beam and 3.5% by Mohan *et al.*[22] for a 15 MV beam, suggesting that it is not necessary to explicitly account for extra-focal scatter for this machine. The profile benchmarks in Sec. III A. provide a quantitative verification of the source size effects.

3. Acquisition of intensity distribution

For each beam in a simulation, the weights of individual elements in the open beam fluence are adjusted by multiplying the fluence grid by a beam-specific intensity grid. An IMRT treatment consists of a series of small fields shaped by the micro-multileaf collimator (mMLC) at each gantry angle. The leaf sequences are obtained from a translation algorithm based on that of Bortfeld *et al.*,[23] which accounts for leaf leakage and transmission and minimizes the tongue-and-groove effect.[24] The algorithm produces a leaf-sequencing file for each gantry angle, and it also provides a beam weight, or index, associated with each set of leaf positions. This index represents the proportion of the total dose that has been delivered when the leaves reach that position. For our treatments the backup jaws remain at 9.8×9.8 cm^2.

The intensity grid for one set of leaf positions is a map of relative transmission values corresponding to the specific mMLC field shape. In order to create the grid, the leaf positions and index values for a beam are read from the sequencing file. For each segment, the mMLC leaf shape is mapped onto a 200×200 grid by assigning every element in the grid the value of the thickness of the corresponding leaf region. The transmission for each element can be found by

$$T(x,y)=\exp(-\mu_w(x,y)*l(x,y)), \tag{1}$$

where $\mu_w(x,y)$ is the linear attenuation coefficient of the material, and $l(x,y)$ is the path length through the mMLC at the position (x,y).

The treatment-specific intensity grid, $I(x,y)$, for a particular gantry angle is calculated from the transmission matrix, $T(x,y)$ by

$$I(x,y)=\sum_{s=1}^{n} T(x,y)_s*i_s, \tag{2}$$

where i_s is the index value for the segment, or the dose proportion delivered in the segment. The product of the intensity grid and the open beam fluence gives the treatment-specific sampling map for the IMRT sequence.

4. mMLC geometry

In order to accurately determine the path length through the mMLC at any point (x,y), we must consider the geometry of the leaves as well as the divergence of the radiation beam. A cross sectional image of the mMLC in the direction perpendicular to leaf motion shows that each leaf is composed of a central core and an edge with two steps on each side, making up the tongue-and-groove, as shown in Fig. 2(a), and including a 0.06 mm gap between neighboring leaves. The nominal leaf width is the sum of the core and the first step of the edge on each side, and the leaf widths are 1.67 mm, 2.50 mm, and 3.05 mm, corresponding to 3 mm, 4.5 mm, and 5.5 mm at isocenter. The average core widths for the three leaves are 1.12 mm, 1.95 mm, and 2.50 mm, respectively, and they are each mapped to 4, 7, and 9 rows in the intensity grid. This represents the thickest portion of a leaf. For all leaves, the average full width of each edge, or the tongue-and-groove, is 0.55 mm, and it is mapped to 2 rows in the intensity grid. Each of these rows includes the contributions from the edges of two neighboring leaves. This allows us to account for interleaf leakage in the model, as well as simulate the effects of leaf sequencing, specifically the tongue-and-groove effect. Small approximations are made in the mapping process because of the fixed matrix size, however the 0.5 mm pixel size at isocenter provides an accurate physical model of the leaves, as demonstrated by our results (Sec. III).

The tip of each leaf is shaped in the vertical direction as shown in Fig. 2(b). The center of the leaf is straight, and beyond this the top and bottom are at an angle of approximately 2.9° relative to the vertical axis. Thus there is a region of approximately 1.1 mm over which the leaf thickness

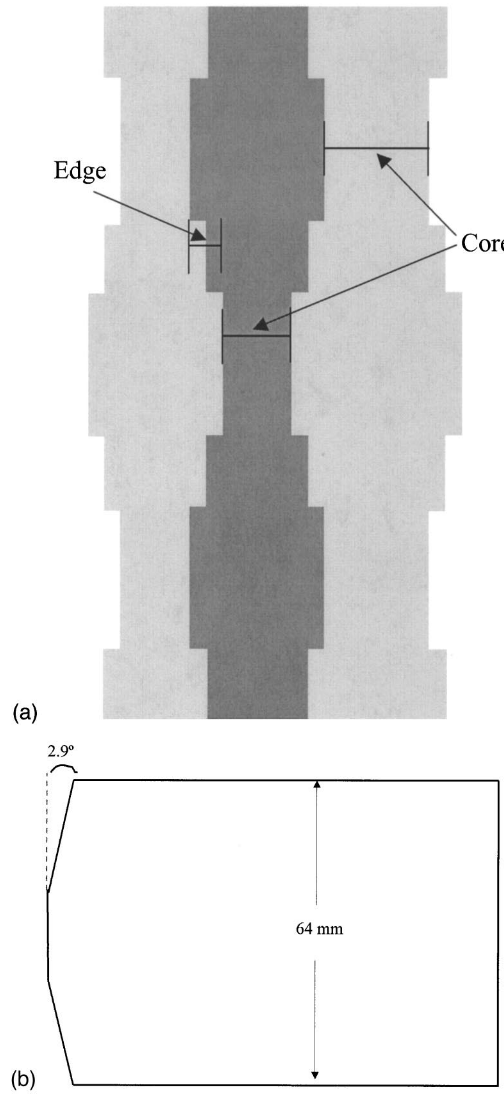

FIG. 2. (a) Simplification of a cross section of mMLC leaves showing the core and edges of two different sized leaves. Nominal leaf widths shown are, from left to right, 3 mm, 3 mm, and 4.5 mm. (b) Side view of the rounded tip of a leaf. The center of the leaf is straight, and beyond this the top and bottom are at an angle of 2.9° relative to the vertical axis.

increases from 2.0 cm at the tip to the full thickness of 6.4 cm. While some IMRT planning systems take the tip shape into account by using an equivalent shift in the position of the field edge,[25,26] we have directly modeled the leaf tip geometry.

5. Path length

The path length through the leaf is initially calculated for the core of the leaf, incorporating the divergence in the direction of leaf motion, as well as the shaped tips of the leaves. The divergence of the radiation beam is accounted for perpendicular to the direction of leaf motion by the truncated pie shape of the leaf bank. For each pixel in the intensity grid, the ray line connecting the source to the pixel is considered. The path length represents the portion of that ray line that passes through a leaf. The intersection of the ray and

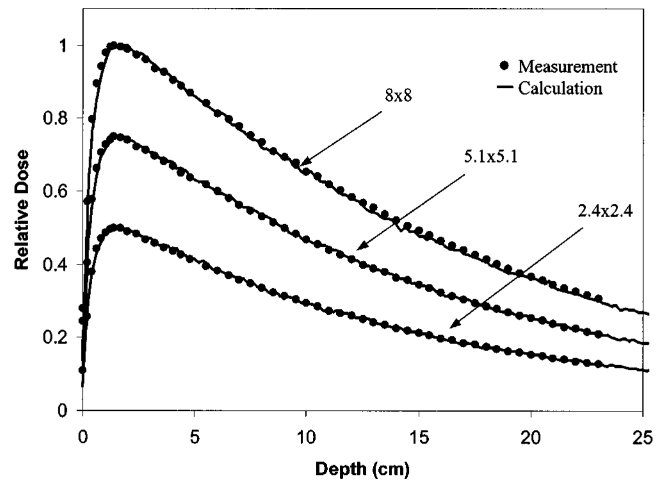

FIG. 3. Comparison of Monte Carlo depth dose calculations versus ion chamber measurements for three field sizes. The curves for the $2.4 \times 2.4\ \mathrm{cm}^2$ and $5.1 \times 5.1\ \mathrm{cm}^2$ fields are scaled by 0.5 and 0.75, respectively, for inclusion on the same graph, and all curves are normalized to $d_{\max}$.

the borders of the core of the corresponding leaf are determined, if any, and the distance between these points is the path length through the core of the leaf.

For pixels that correspond to the edges of the leaves, the core path length is adjusted to account for the tongue-and-groove geometry. The path length through the core is multiplied by the relative thickness of the edge with respect to the core. This factor is 0.60 for the edge nearest the core, and 0.34 for the outside edge of the leaf. A pixel on the edge between two closed leaves will be assigned the sum of the path lengths of the respective leaves. This method produces the path length for each pixel, accounting for the tongue-and-groove and shaped tip geometries of the leaves, as well as interleaf leakage and beam divergence.

6. Attenuation coefficient

As discussed in Sec. II B 2, there is an 8.8% variation in the beam energy across the field due to the flattening filter. This effect is incorporated into the beam-specific intensity grid by varying the linear attenuation coefficient in Eq. (1) based on the pixel position in the field. In the Monte Carlo simulation of the Novalis treatment head, the average energies are tabulated for 20 ring detectors covering the maximum field area. The XCOM database provided by NIST[27] was used to determine mass attenuation coefficients for Tungsten for these average energies. The mMLC is made of a Tungsten alloy of unknown composition. Thus the density of the material was determined from the measured transmission at the central axis, and used to compute linear attenuation coefficients from the XCOM data.

Each of the average energies corresponds to a distance from the central axis (the radius of the appropriate ring detector). A look-up table is created containing the linear attenuation coefficients for these radii. In calculating the transmission for the intensity grid, the distance from the central

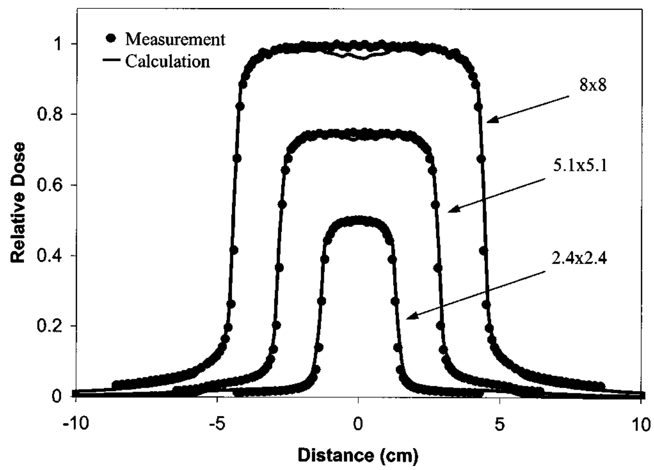

FIG. 4. Comparison of Monte Carlo profile calculations and ion chamber measurements for three field sizes. Curves for the $2.4\times2.4\ \mathrm{cm}^2$ and $5.1\times5.1\ \mathrm{cm}^2$ fields are scaled by 0.5 and 0.75, respectively, for inclusion on the same graph, and all curves are normalized to maximum profile dose.

axis is determined for each pixel, and the linear attenuation coefficient corresponding to the nearest ring is found in the look-up table.

III. RESULTS

A. Benchmarks

The phase space source was benchmarked against standard depth dose and profile ion chamber measurements for the Novalis accelerator. Calculations were done in a $30\times30\times30\ \mathrm{cm}^3$ simulated water phantom for field sizes of $2.4\times2.4\ \mathrm{cm}^2$, $5.1\times5.1\ \mathrm{cm}^2$, and $8\times8\ \mathrm{cm}^2$. We used a cylindrical tally cell with a grid spacing of 2 mm, and low energy cutoffs were 10 keV and 400 keV for photons and electrons, respectively. Figure 3 illustrates a comparison between measured and calculated relative depth dose values for the three benchmark field sizes. Excellent agreement, within 2% of measurement, is seen in all regions of the curves. Figure 4 shows a comparison of measured and calculated profile benchmarks. Agreement is within 2% in the inner beam (dose>90%) and outer beam (dose<10%) regions, and within 2 mm in the penumbral region (10%<dose<90%); thus the profile benchmarks are well within the AAPM Task Group No. 53 criteria for dose comparison.[28] All source calculation points have a 1σ uncertainty of less than 2%.

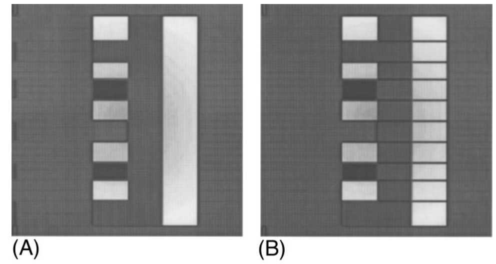

FIG. 6. Monte Carlo sampling maps for leaf sequences A (left) and B (right). The difference in the tongue-and-groove effect between the two sequences is apparent in the sampling maps.

B. Leaf sequencing evaluation

Three examples will demonstrate the accuracy of the phase space model for arbitrary IMRT sequences, and it's effectiveness in evaluating leaf sequencing algorithms. Measurements were made using Kodak X-OMAT V film in a solid water phantom. Monte Carlo simulations were done in a simulated water phantom of the same size, with $2\times2\times2\ \mathrm{mm}^3$ voxel resolution. Low energy cutoffs were 10 keV for photons and 400 keV for electrons.

The first example demonstrates the ability of the model to simulate the effects of leaf sequencing. Figure 5 illustrates this effect with films of two leaf sequences; the only difference between the two sequences is that the one on the left (sequence A) was created to minimize the tongue-and-groove effect and the one on the right (sequence B) was not. The

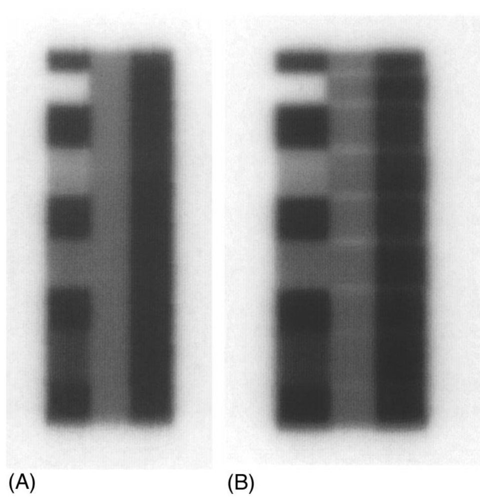

FIG. 5. Film measurements of the tongue-and-groove effect. The sequence on the left (A) minimizes the tongue-and-groove effect, the sequence on the right (B) does not.

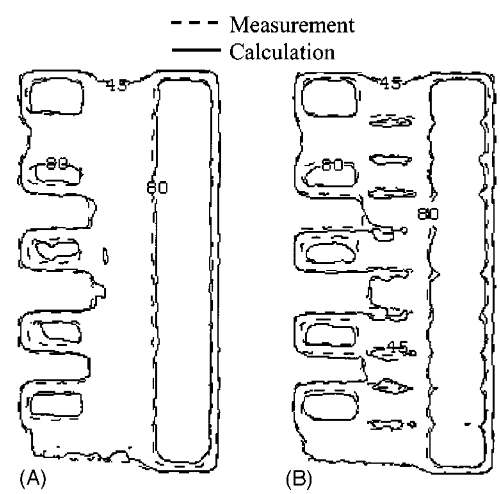

FIG. 7. Comparison of Monte Carlo calculation (solid line) and film measurement (dashed line) for leaf sequences A and B. The 80% and 45% isodose lines are shown.

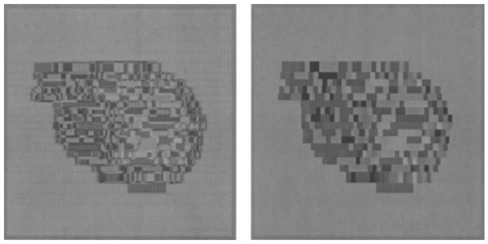

FIG. 8. Sampling maps for a single IMRT beam, incorporating all of the features of the model (left), and using only average leaf transmission (right).

beam-specific fluence maps for these sequences also indicate the differences, as seen in Fig. 6; the interleaf leakage at the edge of the field is present in both maps, and the difference in the leaf sequencing seen on the films is also visible in the sampling maps. Figure 7 indicates that the Monte Carlo dose distributions from the two sequences match the film measurements for the 80% and 45% isodose lines, normalized to maximum.

C. Significance of leaf geometry

A single beam from a five field IMRT prostate plan is used to evaluate the significance of the details that we have incorporated into the model. Two Monte Carlo calculations were done for the sequence, one using the complete model and the other accounting only for the average transmission through the leaves and ignoring the leaf geometry, divergence and energy variation. The resulting intensity grids are shown in Fig. 8, and the comparisons between the Monte Carlo calculations and film measurement are in Fig. 9. The differences in the dose distributions are subtle, but the more accurate model is better able to resolve subtleties in the distribution, particularly at high and low isodoses.

D. IMRT verification—5-field plan

Figure 10 shows the comparison of Monte Carlo calculation and film for a multiple beam IMRT plan. This plan simulates a prostate boost treatment, with five nonopposing IMRT beams at gantry angles of 0°, 60°, 140°, 220°, and 300°. The figure shows the 90%, 50%, and 20% isodose lines for the coronal isocenter slice, normalized to the isocenter. Again, there is excellent agreement between the Monte Carlo simulation and measurement.

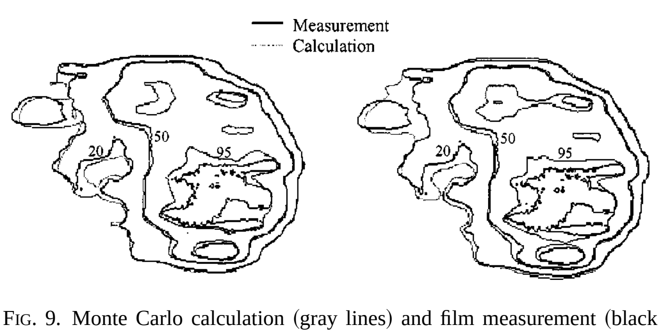

FIG. 9. Monte Carlo calculation (gray lines) and film measurement (black lines) for the single field, incorporating all of the features of the model (left), and using only average leaf transmission (right).

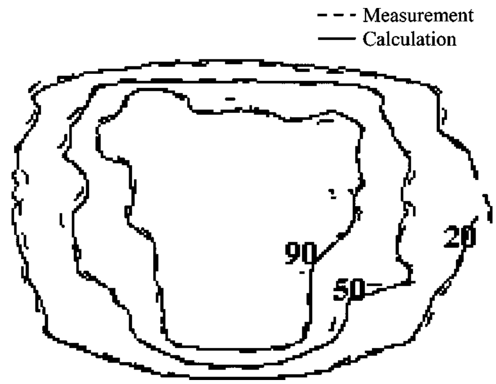

FIG. 10. Comparison of Monte Carlo calculation (solid lines) and film measurement (dashed lines) for a 5 Beam IMRT prostate plan. The 90%, 50%, and 20% isodose lines are shown on the coronal, isocenter slice, normalized to isocenter.

IV. DISCUSSION AND CONCLUSION

A Monte Carlo model has been developed for IMRT, using a Novalis linear accelerator, equipped with an m3 micromultileaf collimator. The modified phase space model accurately simulates arbitrarily shaped static fields as well as IMRT sequences, making it a viable verification technique for IMRT on a linear accelerator with limited field size. We have modeled the multileaf collimator, accounting for the leaf geometry and leaf sequencing effects, beam divergence and the energy variation across the field. The geometry we use is specific to the m3 collimator, but the method of path length calculation could be applied to other collimator geometries.

The source is created by adjusting the discrete fluence weights in the phase space map based on the field shape, which eliminates the inefficient step of calculating particle transport through the leaves. Arbitrary beam weights and gantry, collimator and table angles are also accounted for, allowing for the simulation of complete clinical treatments.

Depth dose and profile benchmarks are found to be within the AAPM Task Group No. 53 acceptability criteria for three field sizes covering the range of clinical fields. IMRT plans with series of irregularly shaped fields are also accurately simulated, including leaf edge and sequencing effects. This model presents a virtual simulation tool for dosimetric verification of clinical IMRT treatments, and it also provides a method of comparing and evaluating leaf sequencing algorithms and optimization techniques.

[a)]Author to whom correspondence should be addressed. Electronic mail: raaronson@radonc.ucla.edu

[1]Intensity Modulated Radiation Therapy Collaborative Working Group, ''Intensity modulated radiation therapy: the state of the art,'' 2001.
[2]P. Andreo, ''Monte Carlo techniques in medical radiation physics,'' Phys. Med. Biol. **36**, 861–920 (1991).
[3]J. J. DeMarco, T. D. Solberg, and J. B. Smathers, ''A CT-based Monte Carlo simulation tool for dosimetry planning and analysis,'' Med. Phys. **25**, 1–11 (1998).
[4]A. Kapur, C. M. Ma, E. C. Mok, D. O. Findley, and A. L. Boyer, ''Monte Carlo calculations of electron beam output factors for a medical linear accelerator,'' Phys. Med. Biol. **43**, 3479–3494 (1998).
[5]C. M. Ma, E. Mok, A. Kapur, T. Pawlicki, D. Findley, S. Brain, K. Forster, and A. L. Boyer, ''Clinical implementation of a Monte Carlo

treatment planning system,'' Med. Phys. **26**, 2133–2143 (1999).

[6] K. R. Shortt, C. K. Ross, A. F. Bielajew, and D. W. Rogers, ''Electron beam dose distributions near standard inhomogeneities,'' Phys. Med. Biol. **1**, 235–249 (1986).

[7] L. Wang, C. S. Chui, and M. Lovelock, ''A patient-specific Monte Carlo dose-calculation method for photon beams,'' Med. Phys. **25**, 867–878 (1998).

[8] J. Deng, T. Pawlicki, Y. Chen, J. Li, S. B. Jiang, and C. M. Ma, ''The MLC tongue-and-groove effect on IMRT dose distributions,'' Phys. Med. Biol. **46**, 1039–1060 (2001).

[9] X. Wang, S. Spirou, T. LoSasso, J. Stein, C. S. Chui, and B. Mohan, ''Dosimetric verification of intensity-modulated fields,'' Med. Phys. **23**, 317–327 (1996).

[10] H. Palmans, F. Verhaegen, F. M. Buffa, and C. Mubata, ''Considerations for modeling MLCs with Monte Carlo techniques,'' *Proceedings from the 13th International Conference, The Use of Computers in Radiation Therapy*, 2000, pp. 458–460.

[11] M. K. Fix, P. Manser, E. J. Born, R. Mini, and P. Ruegsegger, ''Monte Carlo simulation of a dynamic MLC based on a multiple source model,'' Phys. Med. Biol. **46**, 3241–3257 (2001).

[12] T. Pawlicki and C. M. Ma, ''Monte Carlo simulation for MLC-based intensity-modulated radiotherapy,'' Med. Dosim **26**, 157–168 (2001).

[13] P. J. Keall, J. V. Siebers, M. Arnfield, J. O. Kim, and R. Mohan, ''Monte Carlo dose calculations for dynamic IMRT treatments,'' Phys. Med. Biol. **46**, 929–941 (2001).

[14] I. Chetty, J. J. DeMarco, and T. D. Solberg, ''A virtual source model for Monte Carlo modeling of arbitrary intensity distributions,'' Med. Phys. **27**, 166–172 (2000).

[15] I. Chetty, J. J. DeMarco, T. D. Solberg, A. R. Arellano, R. Fogg, and A. V. Mesa, ''A phase-space model for simulating arbitrary intensity distributions for shaped Radiosurgery beams using the Monte Carlo method,'' Radiosurgery **3**, 41–52 (2000).

[16] P. Xia, P. Geis, L. Xing, C. Ma, D. Findley, K. Forster, and A. Boyer, ''Physical characteristics of a miniature multileaf collimator,'' Med. Phys. **26**, 65–70 (1999).

[17] V. P. Cosgrove, U. Jahn, M. Pfaender, S. Bauer, V. Budach, and R. E. Wurm, ''Commissioning of a micro multi-leaf collimator and planning system for stereotactic radiosurgery,'' Radiother. Oncol. **50**, 325–336 (1999).

[18] J. J. DeMarco, I. Chetty, and T. D. Solberg, ''Incorporating conventional treatment planning parameters into a Monte Carlo based dosimetry algorithm,'' Med. Phys. **26**, 1752 (1999).

[19] R. Fogg, I. Chetty, J. J. DeMarco, N. Agazaryan, and T. D. Solberg, ''Modification of a virtual source model for Monte Carlo based IMRT verification,'' *Proceedings from the 13th International Conference, The Use of Computers in Radiation Therapy*, 2000, pp. 420–422.

[20] J. F. Briesmeister, ''MCNP™—A general Monte Carlo N-Particle transport code,'' Los Alamos National Laboratory Report No. LA-12625-M, 1997.

[21] E. L. Chaney, T. J. Cullip, and T. A. Gabriel, ''A Monte Carlo study of accelerator head scatter,'' Med. Phys. **21**, 1383–1390 (1994).

[22] R. Mohan, C. Chui, and L. Lidofsky, ''Energy and angular distributions of photons from medical linear accelerators,'' Med. Phys. **12**, 592–597 (1985).

[23] T. R. Bortfeld, D. L. Kahler, T. J. Waldron, and A. L. Boyer, ''X-ray field compensation with multileaf collimators,'' Int. J. Radiat. Oncol., Biol., Phys. **28**, 723–730 (1994).

[24] N. Agazaryan, T. D. Solberg, A. R. Arellano, and T. J. Paul, ''Leaf sequencing for fluence modulated radiation therapy,'' Med. Phys. **26**, 1139 (1999).

[25] M. Arnfield, J. V. Siebers, J. O. Kim, Q. Wu, P. J. Keall, and R. Mohan, ''A method for determining multileaf collimator transmission and scatter for dynamic intensity modulated radiotherapy,'' Med. Phys. **27**, 2231–2241 (2000).

[26] T. LoSasso, C. S. Chui, and C. C. Ling, ''Physical and dosimetric aspects of a multileaf collimation system used in the dynamic mode for implementing intensity modulated radiotherapy,'' Med. Phys. **25**, 1919–1927 (1998).

[27] M. J. Berger and J. H. Hubbell, ''XCOM: Photon Cross Section Database,'' http://physics.nist.gov/xcom (1999).

[28] B. Fraass, K. Doppke, M. Hunt, G. Kutcher, G. Starkschall, R. Stern, and J. Van Dyke, ''American Association of Physicists in Medicine Radiation Therapy Committee Task Group 53: quality assurance for clinical radiotherapy treatment planning,'' Med. Phys. **25**, 1773–1829 (1998).